Earth Surface Processes and Landforms
Earth Surf. Process. Landforms **28**, 625–644 (2003)
Published online in Wiley InterScience (www.interscience.wiley.com). DOI: 10.1002/esp.471

THREE-DIMENSIONAL FLOW STRUCTURE AND CHANNEL CHANGE IN AN ASYMMETRICAL COMPOUND MEANDER LOOP, EMBARRAS RIVER, ILLINOIS

KELLY M. FROTHINGHAM[1]* AND BRUCE L. RHOADS[2]

[1] *Department of Geography and Planning, Buffalo State College, 1300 Elmwood Avenue, Buffalo, NY 14222, USA*
[2] *Department of Geography, 220 Davenport Hall, University of Illinois, 607 S. Mathews Ave., Urbana, IL 61801, USA*

Received 14 January 2002; Revised 12 June 2002; Accepted 25 July 2002

ABSTRACT

The planform dynamics of meandering rivers produce a complex array of meander forms, including elongated meander loops. Thus far, few studies have examined in detail the flow structure within meander loops and the relation of flow structure to patterns of planform change. This field-based investigation examines relations between three-dimensional fluid motion and channel change within an elongated, asymmetrical meander loop containing multiple pool–riffle structures. The downstream velocity field is characterized by a high-velocity core that shifts slightly outward as flow moves through individual lobes of the loop. For some of the measured flows this core becomes submerged below the water surface downstream of the lobe apexes. Vectors of cross-stream/vertical velocities indicate that skew-induced helical motion develops within the pools near lobe apexes and decays over riffles where channel curvature is less pronounced. Maximum rates of bank retreat generally occur near lobe apexes where impingement of the flow on the outer channel bank is greatest. However, maximum rates and loci of bank retreat differ for upstream and downstream lobes of the loop, leading to increasing asymmetry of loop geometry over time – a finding consistent with experimental investigations of loop evolution. Copyright © 2003 John Wiley & Sons, Ltd.

KEY WORDS: fluvial geomorphology; three-dimensional flow; meandering streams; channel change

INTRODUCTION

The dynamics of meandering rivers are the product of, as yet, incompletely understood interactions among channel planform, bed morphology, sediment transport and three-dimensional (3-D) flow structure. Over time, these dynamics produce various types of bend configurations, including elongated meander loops (Brice, 1974; Hooke, 1995). Early use of the term 'meander loop' in geomorphology was rather nebulous (e.g. Leopold *et al*., 1964: 297), but Brice (1974) defined a loop as any bend that has a chord length, or straight-line distance between inflection points bounding an arc of curvature, greater than the radius of this arc of curvature. This criterion is problematic because it includes meanders that do not curve back upon themselves toward a point of intersection (Figure 1), an essential condition in the dictionary definition of a loop (Anon., 1980). To conform to the dictionary definition, the absolute angles $|\alpha|$ of the channel path relative to the downvalley direction at points of inflection on the flanks, or neck, of a bend should sum to 180° or more before it is considered a loop. Meanders that fail to meet this criterion constitute simple bends. Many meander loops exhibit elongation wherein the chord distance across the neck of the loop is equal to or less than the perpendicular distance from this chord to the apex of the loop (Figure 1). A loop becomes compound when it has two or more offset lobes, or distinct arcs of curvature, on its perimeter (Brice, 1974; Figure 1). These arcs may or may not be separated by intervening straight channel segments. Moreover, many compound loops are asymmetrical, in the sense that each of the multiple arcs of curvature has a different radius of curvature (Brice, 1974; Figure 1).

A hallmark of elongated meander loops is the development of multiple bar forms, especially pool–riffle sequences, within the loop (Hooke and Harvey, 1983). Experimental studies have shown that, in symmetrical

* Correspondence to: K. M. Frothingham, Department of Geography and Planning, Buffalo State College, 1300 Elmwood Avenue, Buffalo, NY 14222, USA. E-mail: frothikm@buffalostate.edu

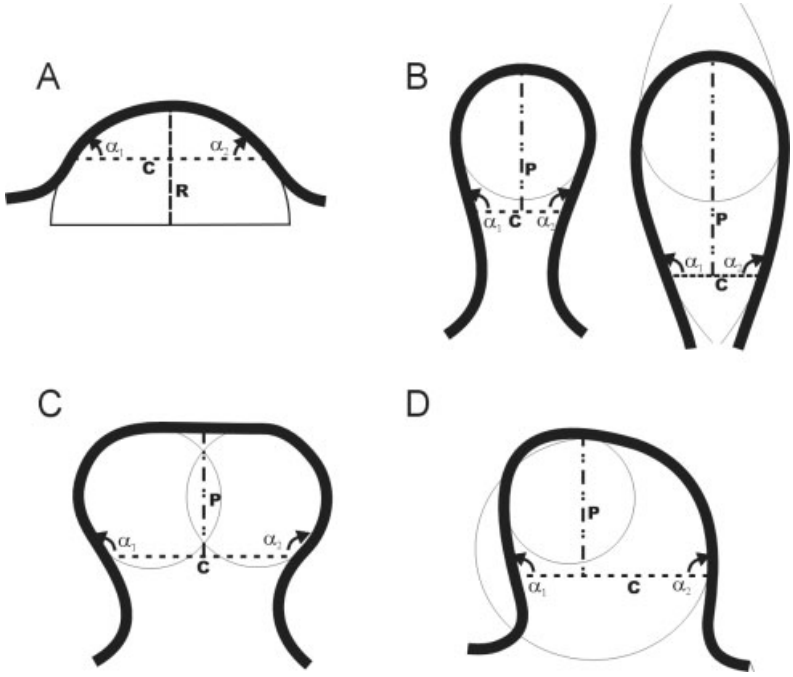

Figure 1. Types of meander bend: (A) a simple meander bend where the chord length C exceeds the radius of curvature R and $|\alpha_1| + |\alpha_2| < 180^o$ (classified as a meander loop by Brice (1974)); (B) elongate symmetrical meander loops with $P > C$ and $|\alpha_1| + |\alpha_2| > 180°$, where P is the perpendicular distance from the chord to the loop apex; (C) symmetrical compound meander loop; (D) asymmetrical compound meander loop. Arcs of curvature indicated by circles or portions of circles

loops, the bed deforms into a systematic series of overlapping morphologic elements known as shingle bars (Whiting and Dietrich, 1993a; (Figure 2). These forms are variants of alternating bar units that develop in straight channels and in sequences of low to moderate amplitude bends with systematic reversal of curvature (Dietrich, 1987; Rhoads and Welford, 1991; Figure 2). In channels with alternating bar units, pools and topographic highs oscillate from one side of the channel to the other through successive units. In low- to moderate-amplitude meanders only a single bar unit is associated with the pool, riffle and point-bar topography within a bend (e.g. Dietrich, 1987; Figure 2). In contrast, high-amplitude loops contain multiple bar units and these bars generally have the same sense of symmetry. Thus, pool position does not oscillate back and forth across the channel from one bar to the next, but all pools are located along the outer bank, multiple point bars are located along the inner bank, and multiple riffles are positioned along the channel centerline (Figure 2). The field investigation by Hooke and Harvey (1983) confirmed that double-headed meanders and other compound loops contain multiple pools and riffles, but did not relate these morphologic elements to bar-unit structure.

A considerable number of process-based field studies have examined patterns of time-averaged flow through meander bends with a single pool, riffle and point bar, i.e. a bar-unit structure (Hey and Thorne, 1975; Dietrich and Smith, 1983; Thorne and Rais, 1984; Thorne *et al*., 1985; Markham and Thorne, 1992), but field measurements of flow structure through meander loops are lacking. Even in studies of simple bends, limitations in measurement technology have required the three-dimensionality of flow to be inferred from, at most, two-dimensional (2-D) measurements of velocity components. Moreover, few of these investigations have attempted to relate patterns of 3-D flow through bends to channel change via bank erosion.

The objectives of this research are to determine the structure of time-averaged 3-D fluid motion within an asymmetrical, compound meander loop and to relate this 3-D flow structure to patterns of channel change via bank erosion. The 3-D structure of the flow is derived from 3-D measurements of velocity components, thereby avoiding the limitation of inferring flow structure from 2-D data. By relating 3-D flow structure to

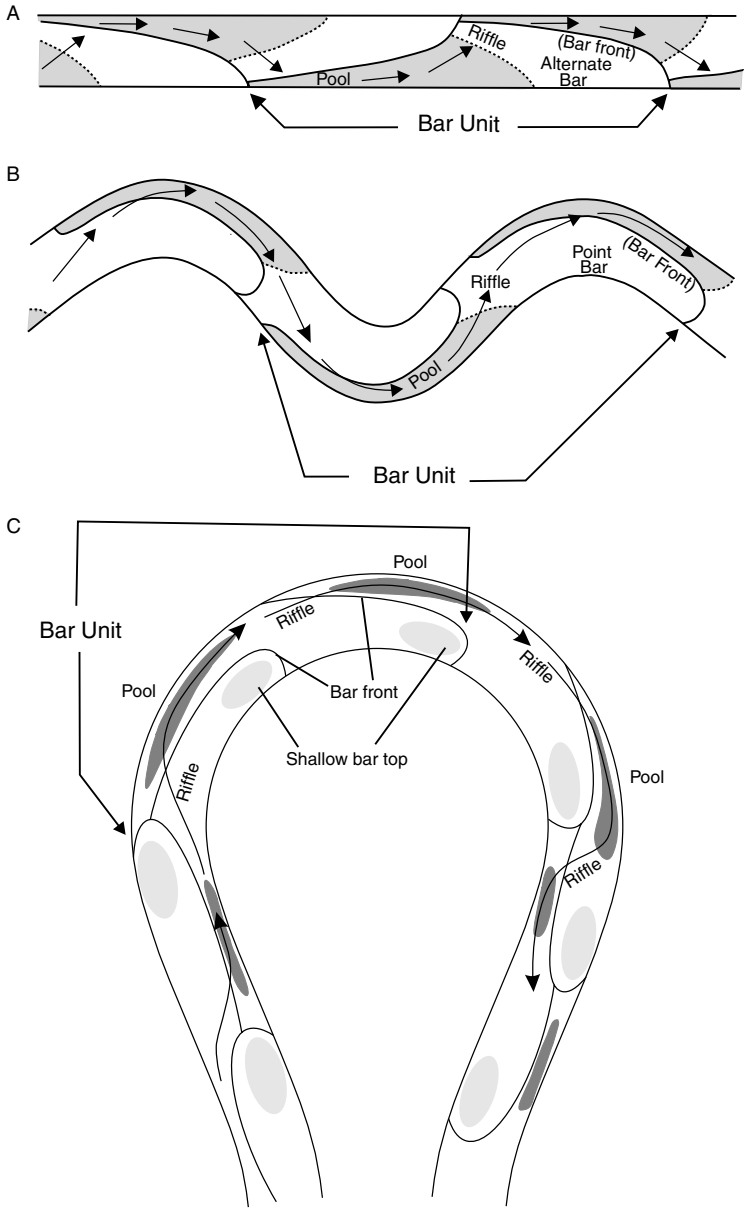

Figure 2. Plan view of bar units in straight (A) and simple meandering (B) channels. Shaded areas correspond to portions of the bed below the mean bed elevation. The highest elevations occur at the portion of the bar unit corresponding to the alternate bar or point bar. (C) Shingle bars in a symmetrical meander loop. Dark shaded areas are pools and light shaded areas are bar tops. Path of thalweg (thread of highest velocity) in each diagram is indicated by arrows (after Dietrich (1987) and Whiting and Dietrich (1993b))

patterns of channel change, the results provide a first step toward unravelling the relation between flow and form within meanders with complex planform characteristics.

STUDY SITE

The study site for this research is an elongated meander loop along the Embarras River in Champaign County, IL (Figure 3). The Embarras River originates on the Urbana moraine at the southern edge of the

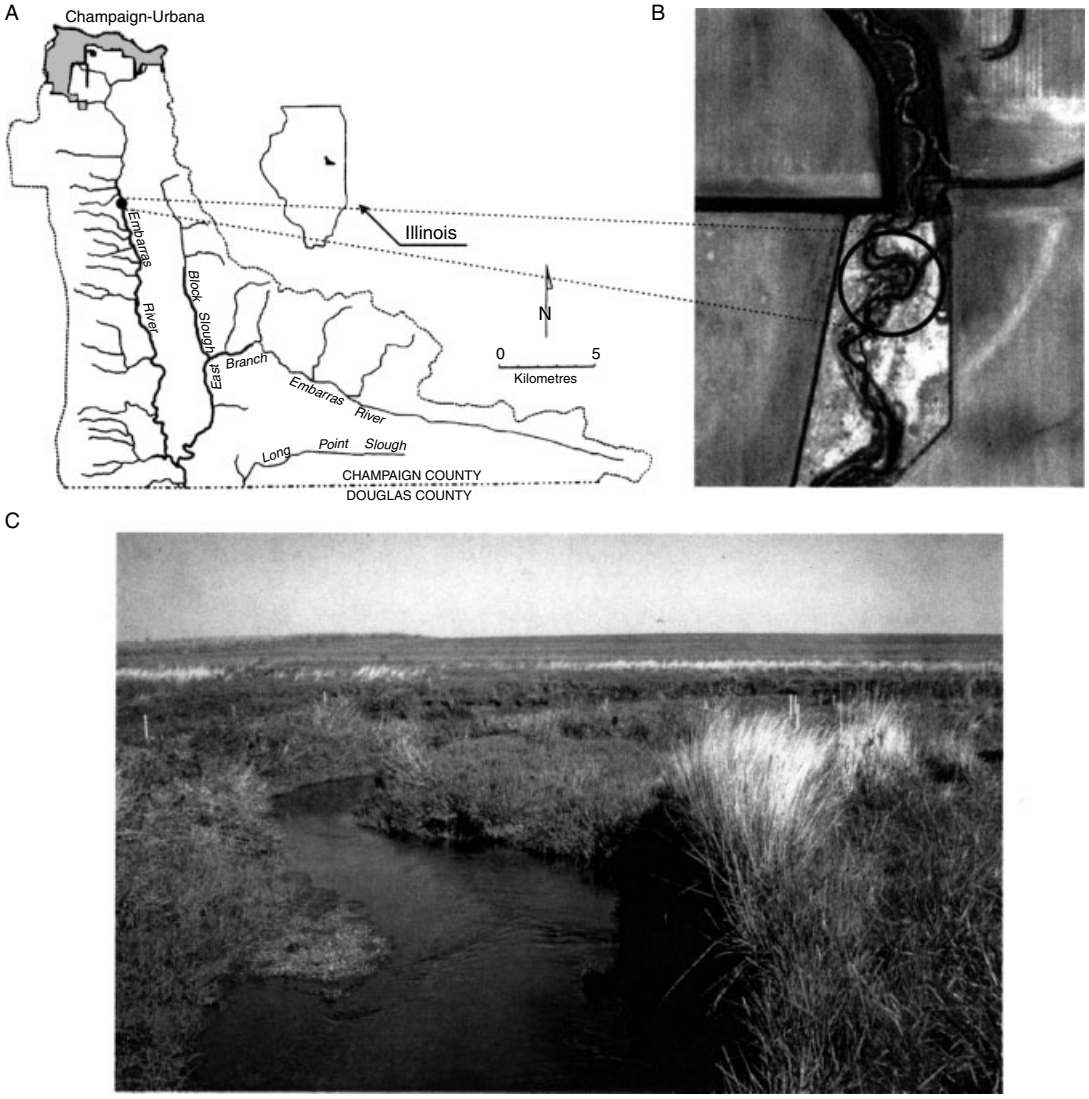

Figure 3. (A) Location of study site. (B) Aerial orthophotograph from April 1998 showing location of the meander loop within the 800 m long meandering reach. (C) Entrance to the meander loop (looking downstream) showing riffle (foreground) and lateral bar along the inner channel adjacent to Pool 1 (middle of photograph)

Champaign–Urbana metropolitan area and flows south between the West Ridge and Philo moraines. These glacial landforms developed approximately 18 000 years ago when the margin of the Lake Michigan lobe of the Laurentide ice sheet retreated to this location from a position further to the south (Hansel and Johnson, 1992). The drainage area of the upper Embarras River watershed at the study site, located about 16 km south of Champaign–Urbana, IL, is 57 km^2. The gradient of the river at the study site is 0·008 m m^{-1}.

Over the past 150 years, the Embarras River has been subjected to repeated channelization for the purpose of land drainage, and many sections of the river have a highly modified form consisting of straight channels with trapezoidal cross-sections (Rhoads and Urban, 1997; Urban, 2000; Frothingham, 2001). The study site is situated within an 800 m section of the Embarras River that has not been channelized since at least the 1930s (Figure 3). This section of the river represents one of the few locations where channel morphology appears to be fully adjusted to prevailing hydrologic conditions and does not include any morphological remnants of

past channelization. Within this 800 m long reach the channel has a meandering planform with a complex assemblage of meander bends and elongate meander loops (Figure 3). It also has a natural cross-sectional morphology with well-developed pool–riffle sequences (Figure 3). Bed material consists of sand and fine gravel.

The meander loop at the study site is approximately 95 m in length. Bankfull channel width ranges from 13·0 to 18·0 m and bankfull depth is between 1·0 and 2·0 m. Absolute values of angular deviation $|\alpha|$ from the downvalley direction are approximately 110°at the loop entrance and 90° at the loop exit (Figure 3). The loop has an asymmetrical, compound planform characterized by three distinct arcs of curvature, all of which have different radii of curvature (Figure 4). Two of the arcs conjoin within the upstream limb of the loop, whereas the second and third arcs meet near the loop apex (Figure 4). This arrangement of arcs of curvature produces two distinct lobes within the loop: an upstream asymmetrical lobe and a downstream symmetrical lobe. The two-lobe form is a loop configuration commonly referred to as a double-headed meander (Hooke, 1995).

Bed morphology within the asymmetrical loop is characterized by multiple pool–riffle–point-bar sequences related to spatial variations in channel morphology and curvature (Figure 4). The pattern of pools and riffles is generally consistent with results of erodible-bed experimental studies of symmetrical loops (Whiting and Dietrich, 1993b). Multiple pools and riffles develop in symmetrical loops in conjunction with deformation of the bed into a series of shingle-like bar units. Morphological features at the field site include a pool at the loop entrance (Pool 1), a riffle upstream of the first lobe of the loop (Riffle 1), a pool near the apex of this lobe (Pool 2), a riffle within the relatively straight section between the two lobes (Riffle 2), a pool near the apex of the downstream lobe (Pool 3), and a riffle at the exit of the loop (Riffle 3; Figure 4). The positioning of the pools is similar to that which develops in symmetrical loops with a sinuosity of 2·69 and bend inflection angles of 100°(Whiting and Dietrich, 1993b; Figure 2). The double-headed loop along the Embarras River has a sinuosity of about 2·3 and angles of inflection of approximately 100°. The positions of the point bars in the loop are relatively stable, a finding consistent with Whiting and Dietrich's (1993b) results, but the topographical structure of these bars is not as clearly defined as that of the shingle bars in Whiting and Dietrich's (1993b) experiments. In particular, the point bars at the field site lack well-defined bar fronts, or curving slip faces, at their downstream ends (Figure 4).

Bed material within the loop is generally coarsest at the riffles and within the thalweg of the pools (unimodal gravel; Figure 5). Glacial till is exposed within the deepest parts of pools close to the outer bank, suggesting that these areas are swept clear of alluvial sediment. Point bars in each lobe are composed either of bimodal sand and gravel (upstream of apex) or unimodal sand (downstream of apex). Bed material texture within the upstream and downstream lobes of the loop does not exhibit a crossover of the coarsest bed material from the inner bank upstream of the lobe apex to the outer bank downstream of the apex, such as that documented in simple meander bends (e.g. Dietrich, 1987). The lack of crossover in sediment texture suggests that the zone of maximum bed shear stress of transport-effective flows is located between the channel midpoint and the outer bank throughout the loop.

METHODOLOGY

The 3-D velocity data were collected within the elongated loop during three separate 2 day measurement campaigns: 5 and 8 June 1998 (campaign 1); 18 and 24 June 1998 (campaign 2); and 27 and 28 July 1998 (campaign 3). The three campaigns correspond to three different sets of hydrological conditions (Table I). Water levels were 41–52% of the maximum bankfull depth (MBD) during campaign 1 (stage: 8·78–8·98 m), 55–64% of MBD during campaign 2 (stage: 9·04–9·20 m), and 33% of MBD during campaign 3 (stage: 8·62–8·64 m). Although hydraulic conditions changed somewhat between the two days of measurements for each campaign, these differences are less than the differences in hydraulic conditions among the campaigns. Thus, for the purpose of analysis, 3-D velocity measurements for each campaign are treated as a single set of data. Although velocity magnitudes will be affected somewhat by changes in discharge, the patterns of flow, the focus of this study, should remain similar for slight changes in stage.

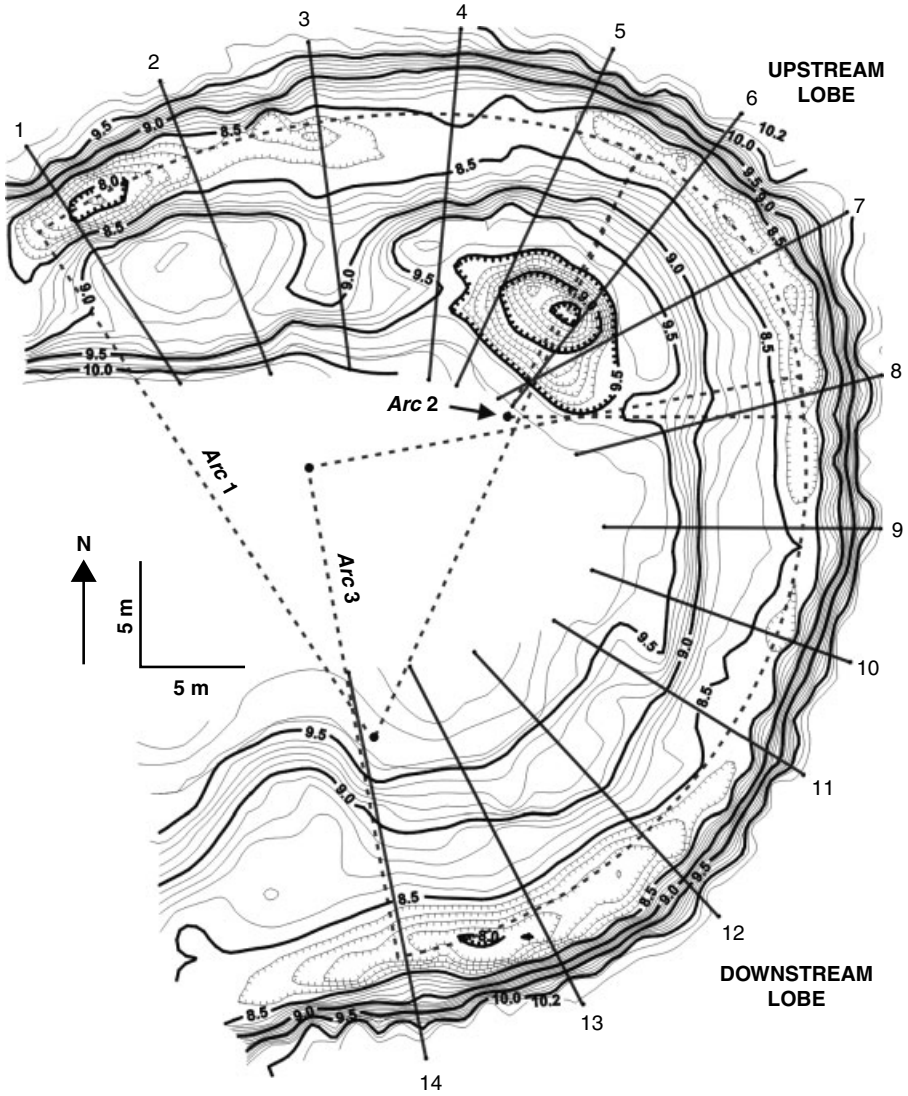

Figure 4. Topographic map of the field site (contour interval 0·1 m; arbitrary datum: 10 m) showing arcs of curvature, monumented cross-sections and upstream and downstream lobes

Velocity measurements were obtained at subsets of 14 cross-sections oriented orthogonally to the local pattern of channel curvature. The logistics of the measurements constrained the collection of data to between three and five cross-sections per day or six to ten cross-sections per sampling campaign. Upstream cross-sections were sampled the first day, followed by downstream cross-sections on the second day.

An acoustic doppler velocimeter (ADV) provided information on downstream (u), vertical (w), and cross-stream (v) velocity components at each cross-section. The ADV uses acoustic sensing techniques to measure flow in three dimensions with a velocity resolution of 0·1 mm s^{-1}. The in-stream measurement scheme involves mounting the ADV probe to a custom-built wading rod that, in turn, is attached to steel taglines stretched tautly between iron pipes at the endpoints of the monumented cross-sections. After the rod is attached to the steel cable, it is plumbed using a rod level to ensure that the vertical axis of the sensor is parallel to the vertical plane of the cross-section. Velocities were measured at two to eight locations over depth at six to eight verticals within a cross-section, resulting in an array of 40 to 50 sampling locations per

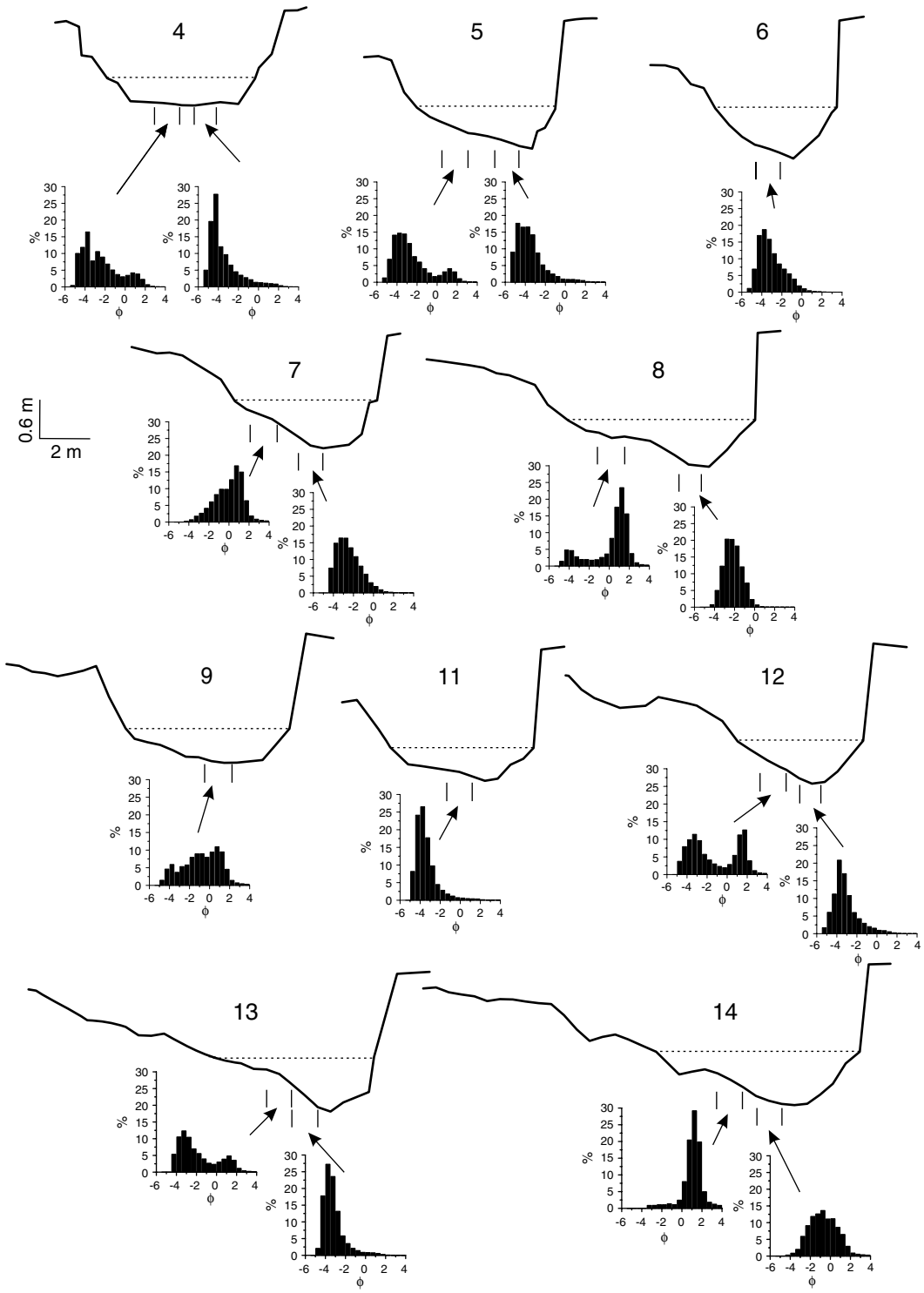

Figure 5. Channel geometry and particle-size distributions of bulk samples of sediment from the upper 10 cm of the channel bed at cross-sections 4–14 within the meander loop

Table I. Summary of hydraulic characteristics for the meander loop[a]

Cross-section	Date	Q (m^3 s^{-1})	w (m)	d (m)	Cross-sectional area (m^2)	v (m s^{-1})	Stage (m)
Measurement campaign 1: 5 and 8 June 1998							
4	5 June	0·78	5·8	0·36	2·09	0·34	8·93
5		0·79	5·3	0·41	2·17	0·33	8·96
6		0·94	4·8	0·52	2·50	0·32	8·98
7		0·97	5·6	0·52	2·91	0·33	8·98
8		0·81	7·3	0·39	2·85	0·28	8·95
9	8 June	0·46	6·4	0·28	1·79	0·24	8·78
11		0·45	5·6	0·27	1·51	0·32	8·78
12		0·47	4·9	0·30	1·47	0·32	8·78
13		0·50	6·5	0·46	2·99	0·22	8·78
14		0·53	8·0	0·41	3·28	0·14	8·78
Measurement campaign 2: 18 and 24 June 1998							
5	18 June	2·37	6·2	0·73	4·53	0·52	9·21
6		2·55	7·8	0·81	6·32	0·53	9·20
7		2·24	6·3	0·75	4·73	0·47	9·18
12	24 June	1·92	5·5	0·60	3·30	0·58	9·08
13		1·84	7·0	0·54	3·78	0·33	9·06
14		1·79	9·7	0·67	6·50	0·21	9·04
Measurement campaign 3: 27 and 28 July 1998							
4	27 July	0·17	4·7	0·19	0·89	0·22	8·64
5		0·19	4·9	0·27	1·32	0·18	8·64
6		0·21	4·6	0·33	1·52	0·13	8·64
7		0·16	4·4	0·43	1·89	0·13	8·64
8		0·19	4·3	0·29	1·25	0·17	8·64
9	28 July	0·16	3·8	0·23	0·87	0·25	8·62
11		0·17	4·5	0·19	0·86	0·28	8·62
12		0·16	6·1	0·25	1·53	0·17	8·62
13		0·17	4·4	0·31	1·36	0·11	8·62
14		0·18	7·3	0·40	2·92	0·05	8·62

[a] Q: discharge; w: width of the water surface; d: mean cross-section depth; v: depth-averaged downstream velocity.

cross-section. Measurements of u, v and w were obtained at a frequency of 25 Hz over a sampling interval of 60–90 s.

Data analysis consisted of computing time-averaged downstream (U), cross-stream (V) and vertical (W) velocities as well as cross-stream/downstream (θ_{uv}) and vertical/downstream (θ_{uw}) vector angles for each measurement location, where

$$\theta_{uv} = \arctan(V/U) \tag{1}$$

$$\theta_{uw} = \arctan(W/U) \tag{2}$$

Because the objective of this study is to explore changes in flow structure at fixed cross-sections with changing stage (e.g. Rhoads and Kenworthy, 1995), rather than to compute force–balance relations (e.g. Dietrich and Smith, 1983), no rotation of cross-section orientations was performed prior to data analysis. Time-averaged 3-D velocities were used to generate depth-averaged 2-D vector plots of downstream and cross-stream velocity components for the set of cross-sections. These plots reveal the general pattern of water movement through the reach. To illustrate in detail the 3-D structure of the flow, contour plots of downstream velocity and vector plots of cross-stream/vertical velocity components were produced for each cross-section. Contours of downstream

velocity were interpolated manually rather than using kriging or other computer-based interpolation schemes, because such schemes could not accurately account for the severe spatial anisotropy in some of the data.

Water stage was monitored within the elongated meander loop during each velocity measurement campaign using two ultrasonic sensors, one at the upstream end of the loop and the other at the downstream end of the loop. A Campbell 21X datalogger was used to sample the sensors, which ultrasonically measure the distance from the sensor head to the water surface at 1 s intervals over a sampling duration of 60–90 s. This sampling was conducted in conjunction with the velocity measurements and the datalogger computed average water-surface elevations for each set of these measurements.

In addition to the velocity measurements, repeat surveys of the 14 channel cross-sections were conducted between 1997 and 1999 to document spatial patterns of erosion and deposition within the loop. Information derived from the surveys provides an objective basis for relating patterns of 3-D flow to patterns of channel change.

RESULTS

Pattern of depth-averaged vectors

Depth-averaged 2-D vectors for the three measurement campaigns reveal the general paths of the flow through the meander loop for different hydrological conditions (Figure 6). At the entrance to the upstream lobe (cross-sections 4 and 5), vectors are generally oriented toward the outer bank over the entire width of the channel. The point bar within this lobe deflects flow along the inner bank outward, leading to flow convergence within the upstream end of the pool (cross-section 6), but vectors at this location are still generally oriented toward the outer bank. Downstream of the lobe apex (cross-section 7) the vectors become aligned more closely with the channel direction, but they also exhibit a divergent pattern for moderate to high flows (campaigns 1 and 2). The cross-stream pattern of vector magnitudes is somewhat asymmetrical at the lobe entrance and this asymmetry increases slightly around the lobe, indicating a progressive shift in the locus of maximum velocity toward the outer bank.

Between the two lobes, velocity vectors for campaigns 1 and 3 are generally aligned with the channel direction (Figure 6); no velocity measurements were obtained in this section of the loop during campaign 2. Slight divergence of flow is evident over Riffle 2, with the strongest divergence at the upstream part of the riffle (cross-section 9) during campaign 1 and at the downstream part of the riffle (cross-section 11) during campaign 3. Flow converges over the downstream part of the riffle during campaign 1 as it approaches the point bar along the inner bank.

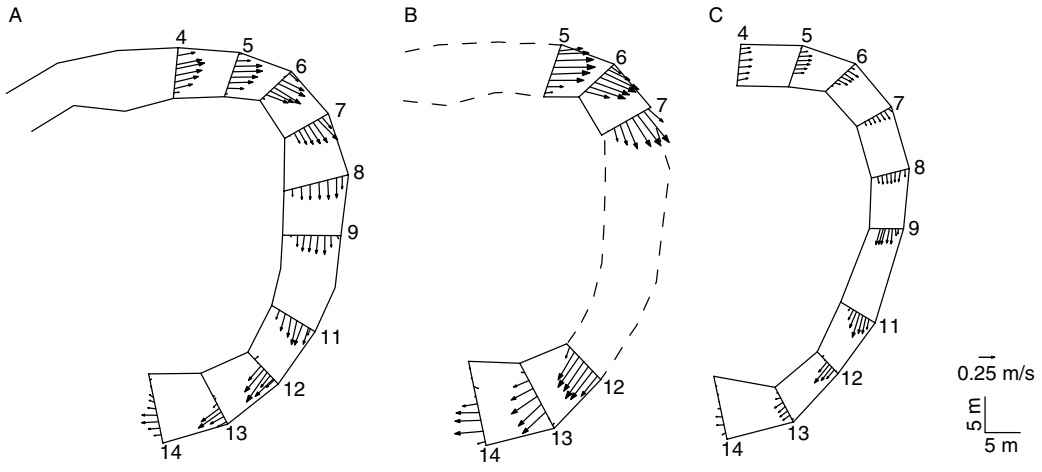

Figure 6. Depth-averaged velocity vectors for (A) campaign 1, 5 and 8 June, (B) campaign 2, 18 and 24 June, and (C) campaign 3, 27 and 28 July 1998

Within the downstream lobe, depth-averaged vectors generally parallel the channel direction, except for vectors near the apex of the lobe (cross-section 13) for campaign 2, which are skewed toward the outer bank. Moreover, the symmetrical cross-stream pattern of vector magnitudes at Riffle 2 is progressively transformed into an asymmetrical pattern within the lobe with the largest vectors located near the outer bank. The protruding point bar at the entrance to the downstream lobe strongly influences the pattern of flow along the inner bank. During campaigns 1 and 3, lateral deflection of the flow toward the outer bank by the point bar produces a small region of recirculating flow over the point bar face (cross-sections 12 and 13). This deflection, along with the abrupt increase in flow width downstream of the lobe apex, results in a sizable region of separated flow in the lee of the point bar (cross-section 14). The flow also markedly diverges in response to channel widening. During campaign 2, the increased depth of flow prevents the development of recirculation over the point-bar face, but the region of separated flow is still present along the inner bank downstream of the point bar.

Pattern of downstream velocity

The general pattern of downstream velocity consists of a high-velocity core surrounded by diminishing velocities toward the channel bed and banks, a pattern typical of that for flow in an open channel (Figure 7). As flow moves through the loop, the position of the high-velocity core within the channel cross-section and the symmetry of the pattern of decreasing velocity away from this core vary with channel curvature and changes in bed morphology. Upstream of the first lobe at Riffle 1 (cross-section 4), the pattern of downstream isovels is symmetrical, with the high-velocity core located in the centre of the channel near the water surface. As flow moves into Pool 2 and around the apex of the upstream lobe (cross-sections 5–7), the high-velocity core shifts toward the outer bank. For campaign 1, the core also becomes submerged beneath the surface near the base of the outer bank. The magnitude of the high-velocity core remains fairly constant through this portion of the loop for the two highest flows (campaigns 1 and 2), but a pronounced deceleration is evident for campaign 3 as the shallow flow moving over Riffle 1 enters Pool 2.

Changes in stage between dates of measurement complicate interpretations of velocity relations over Riffle 2 between the lobes; but, both for campaign 1 and campaign 3, the magnitude of the high-velocity core increases from the upstream end of this riffle to the entry to Pool 3 (cross-sections 8–12). The core remains displaced slightly toward the outer bank over Riffle 2 for campaign 1, but it shifts toward the inner bank for campaign 3. For all three campaigns, flow moving past the point bar in the downstream lobe (cross-section 12) decelerates as it enters the deepening Pool 3 and the widening channel downstream of the point bar (cross-sections 13 and 14). A submerged high-velocity core develops near the base of the outer bank during the moderate and high flows (campaigns 1 and 2), and the locus of this submerged core within the downstream lobe is shifted downstream for the high flow relative to its position for the moderate flow. Negative downstream velocities, corresponding to regions of separated, recirculating flow, are evident along the inner bank over the point bar face for campaigns 1 and 3 (cross-sections 12 and 13), and downstream of the lobe apex in the lee of the point bar for all three campaigns (cross-section 14).

Pattern of velocity components in the cross-stream plane

Patterns of vectors of cross-stream/vertical velocity components illustrate that flow through the reach is 3-D with pronounced helicity in the pools at the lobe apexes (Figure 7). At the entrance to the upstream lobe (cross-sections 4 and 5), vectors are uniformly directed toward the outer bank at all verticals except the ones located closest to this bank. Although this pattern in part reflects skewing of the cross-section relative to the channel direction, the depth-averaged 2-D vectors confirm that flow for all three campaigns is directed toward the outer bank at this location (Figure 6). Within Pool 2 (cross-sections 6 and 7), vectors from the water surface to approximately 0·5 m above the bed are oriented toward the outer bank and downward toward the bed near the outer bank. Conversely, vectors near the bed within Pool 2 are oriented inward and upward over the point-bar face. This opposing pattern of vector orientations near the surface and bed is indicative of helical motion of the flow within the pool.

The magnitude of cross-stream/vertical vectors in Pool 2 increases with rising flow stage, suggesting that the strength of helicity also intensifies with increases in stage. A rotational pattern of vector orientations is

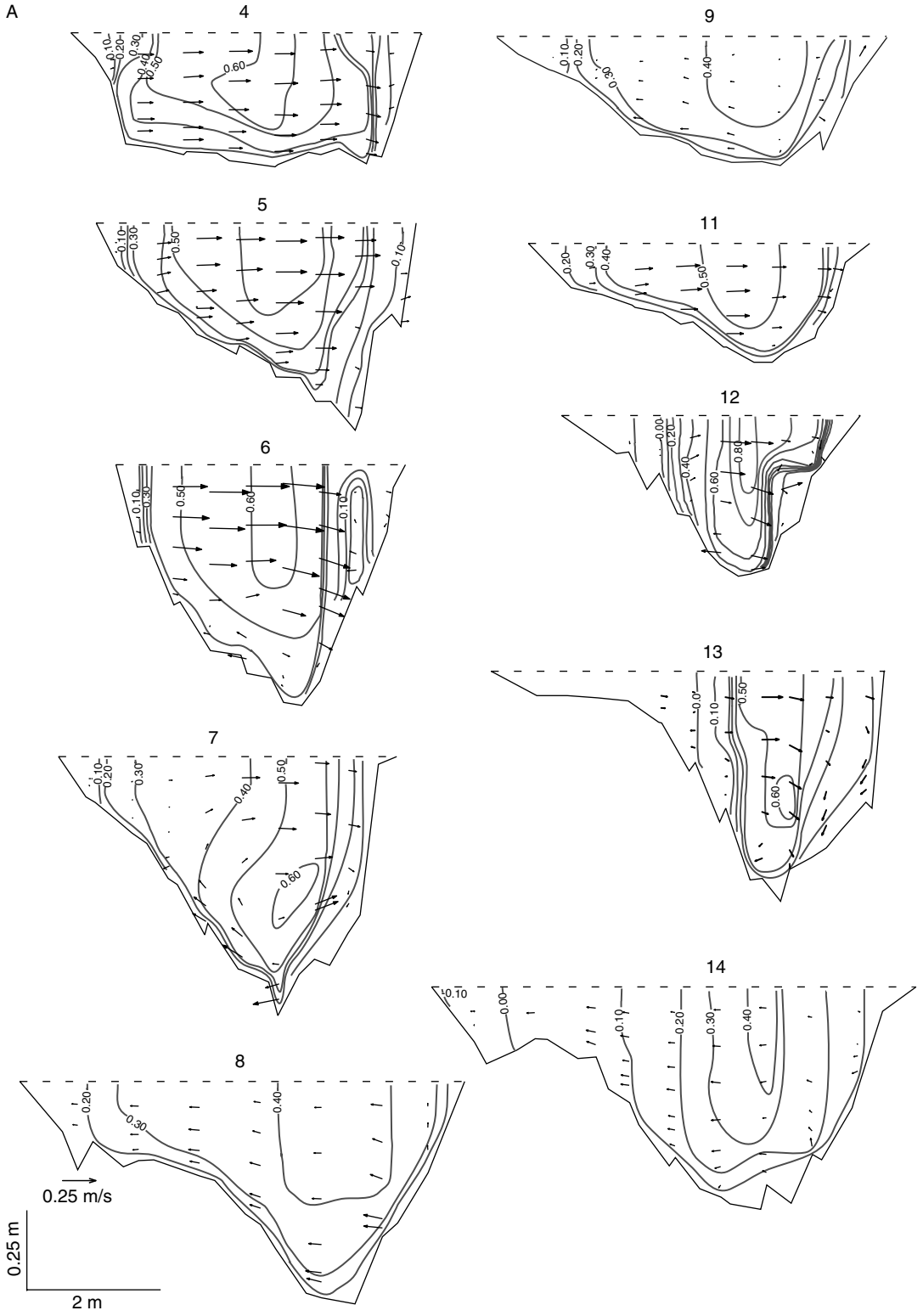

Figure 7. Downstream isovels and vectors of cross-stream/vertical velocity components velocities for (A) campaign 1, 5 and 8 June, (B) campaign 2, 18 and 24 June, and (C) campaign 3, 27 and 28 July 1998

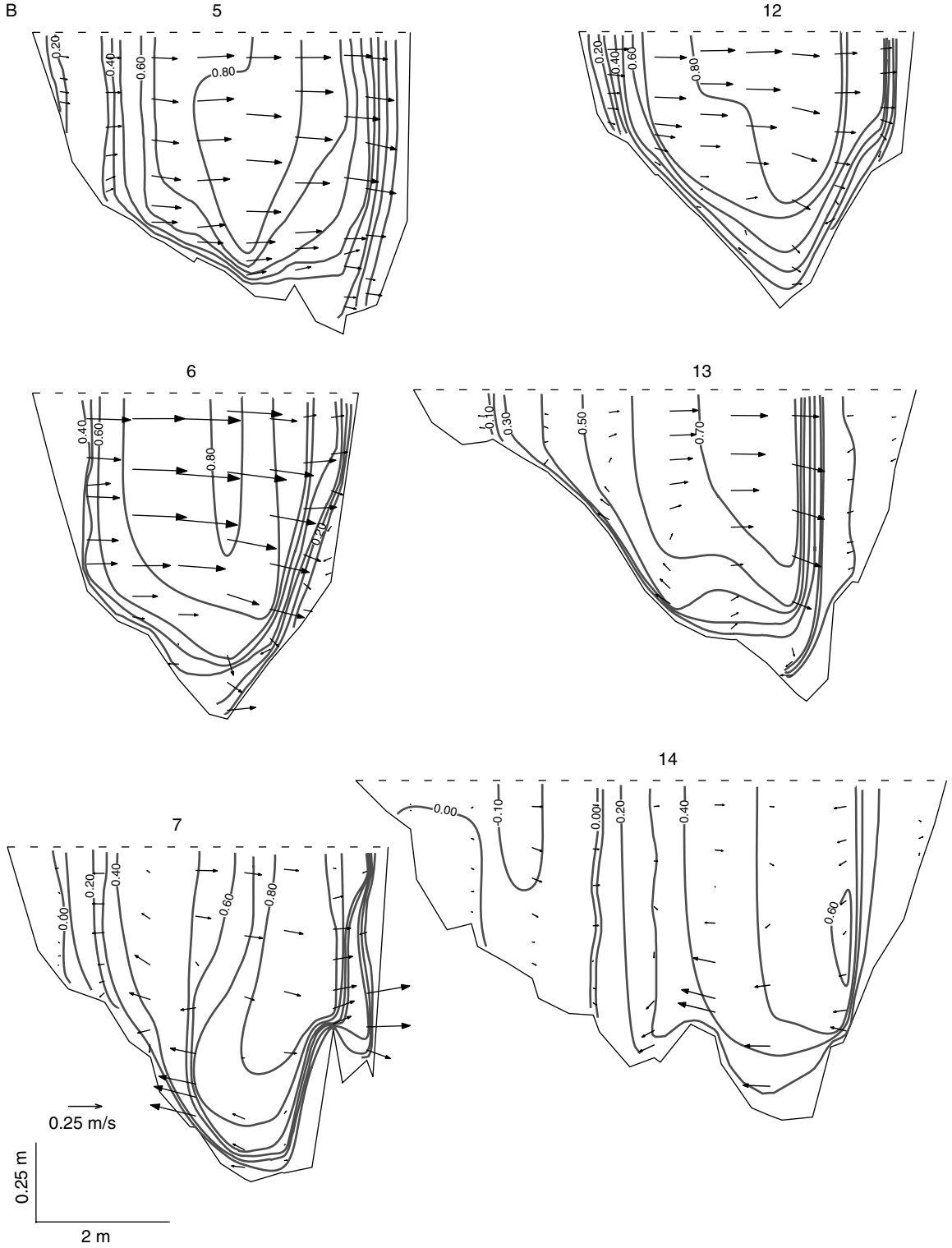

Figure 7. (*Continued*)

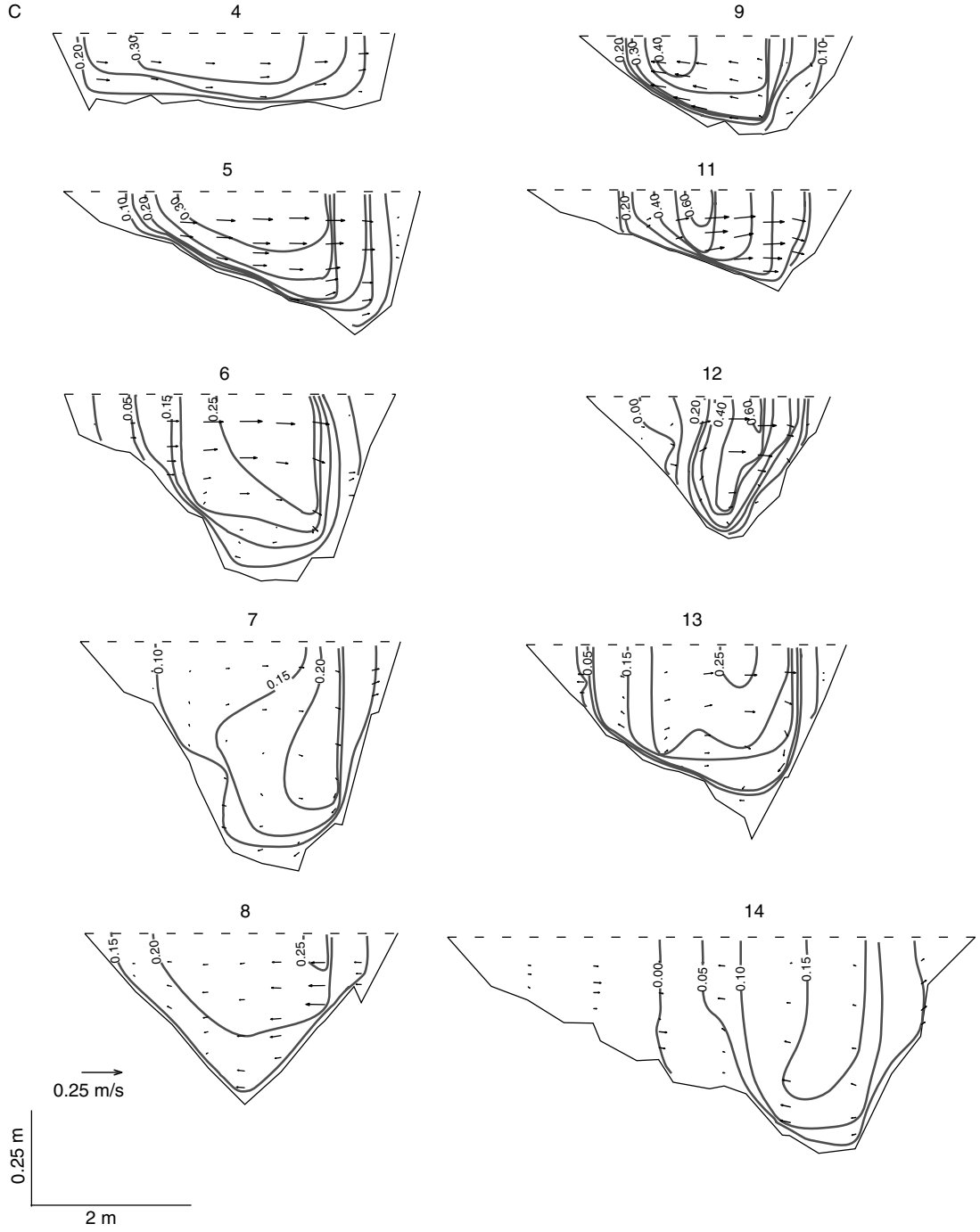

Figure 7. (*Continued*)

best developed immediately downstream of the lobe apex (cross-section 7) for moderate- and low-flow stages (campaigns 1 and 3). At the high stage (campaign 2), the strong outward orientation of depth-averaged and cross-stream/vertical vectors near the lobe apex (cross-section 6; Figure 7) indicates that the flow collides with the bank at an oblique angle, resulting in abrupt reversal of flow near the bed downstream of the apex

(cross-section 7). The pattern of 3-D fluid motion immediately adjacent to the outer bank for the high-stage event (cross-section 7) is complicated by irregular topography associated with failed blocks of bank material. The development of intense helicity within the upstream lobe produces systematic differences in values of θ_{uv} of as much as 50 to 60° over depth.

Helicity is not apparent in the cross-stream plane between the bend apexes for campaigns 1 and 3 (cross-sections 8 and 9). The alignment of depth-averaged vectors with the path of the channel at the exit of Pool 2 (cross-section 8; Figure 6) indicates that the inward orientation of cross-stream/vertical vectors at this location (Figure 7) largely reflects skewing of the cross-section relative to the path of the flow, rather than a net flux of fluid toward the inner bank. Between the two lobes (cross-section 9), weak divergence of flow over Riffle 2 is confirmed by opposing orientations of small-magnitude vectors on each side of the channel.

At the entrance to the downstream lobe (cross-section 11), vectors in the cross-stream plane become directed uniformly toward the outer bank. Opposing patterns of vector orientation over depth through the lobe apex (cross-sections 12 and 13) provide evidence for the redevelopment of helical motion of the flow. This pattern corresponds to differences in values of θ_{uv} of 50–60° over depth. Vertical motion is quite pronounced near the outer bank, with vectors in the cross-stream plane directed nearly orthogonal to the bed, whereas over the point-bar face the fluid near the bed moves inward and upward. As in the upstream lobe, the strength of helicity, as indicated by the magnitudes of cross-stream/vertical vectors, appears to increase with increasing stage.

Abrupt widening of the channel downstream of the lobe apex (cross-section 14) leads to rapid decay of helicity, especially for the low and moderate flows (campaigns 1 and 3). An opposing pattern of vectors over depth is apparent within the downstream portion of Pool 3 for the high flow (campaign 3), but this pattern is confined to the channel thalweg. Vectors within the zone of flow separation along the inner bank are small and unidirectional, suggesting that the pattern of weak fluid recirculation in this separation zone is consistent over depth.

Spatial patterns of erosion and deposition

Repeat surveys of the 14 monumented cross-sections over a 2 year period show that erosion and deposition were most active at the entrance to the loop and at, or near, the apexes of the upstream and downstream lobes of the loop (Figure 8). Changes in Pool 1 at the entrance to the loop involved a decrease in pool depth of about 0·5 m and an increase in pool width of about 2·5 m. Widening of the thalweg at the upstream end of Pool 1 was associated mainly with lateral erosion of the bar platform along the inner bank. At the downstream end of Pool 1 (cross-section 2) the thalweg increased in depth by about 0·33 m and widened by about 2 m. Widening of the thalweg at this location reflected lateral retreat of the outer bank. Between Pool 1 and Riffle 1 (cross-section 3), a distinct depositional mound about 0·20 m high developed along the inner bank and the toe of the outer bank retreated by about 2 m. Channel change at Riffle 1 (cross-section 4) involved about 1 m of lateral accretion along the toe of the inner bank and deepening of the thalweg by 0·20 m, but the position of the outer bank remained stable. The net effect of erosion and deposition at the loop entrance was to increase the obliquity of the thalweg alignment relative to the outer bank. Much of this change in morphology had already occurred by 5 June, the date of the first velocity measurements in the reach, and helps to explain why the overall path of the flow at Riffle 1 (cross-section 4) is oriented toward the outer bank (Figure 6). Reshaping and realignment of the channel at the loop entrance most likely resulted from gradual downstream migration of the sharp bend immediately upstream from this location (Figure 3).

From the entrance to Pool 2 (cross-section 5) to the exit of the loop (cross-section 14), changes in channel morphology are characterized by lateral retreat of the outer bank and accretion along the inner bank (Figure 8). Bank retreat is most pronounced at or near the apexes of the upstream and downstream lobes (cross-sections 6–8 and 12–14). Erosion in the upstream lobe is greatest slightly upstream of the apex (cross-section 6). The amount of erosion increases progressively around the downstream lobe, with the highest rates in the loop, on average 2 m per year, occurring along the outer bank of the downstream limb (cross-section 14).

Accretion along the inner bank also is greatest within the two lobes. Deposition within the upstream lobe is distributed over the entire inner bank, but generally is thin (<0·2 m; Figure 9). Sediments deposited near

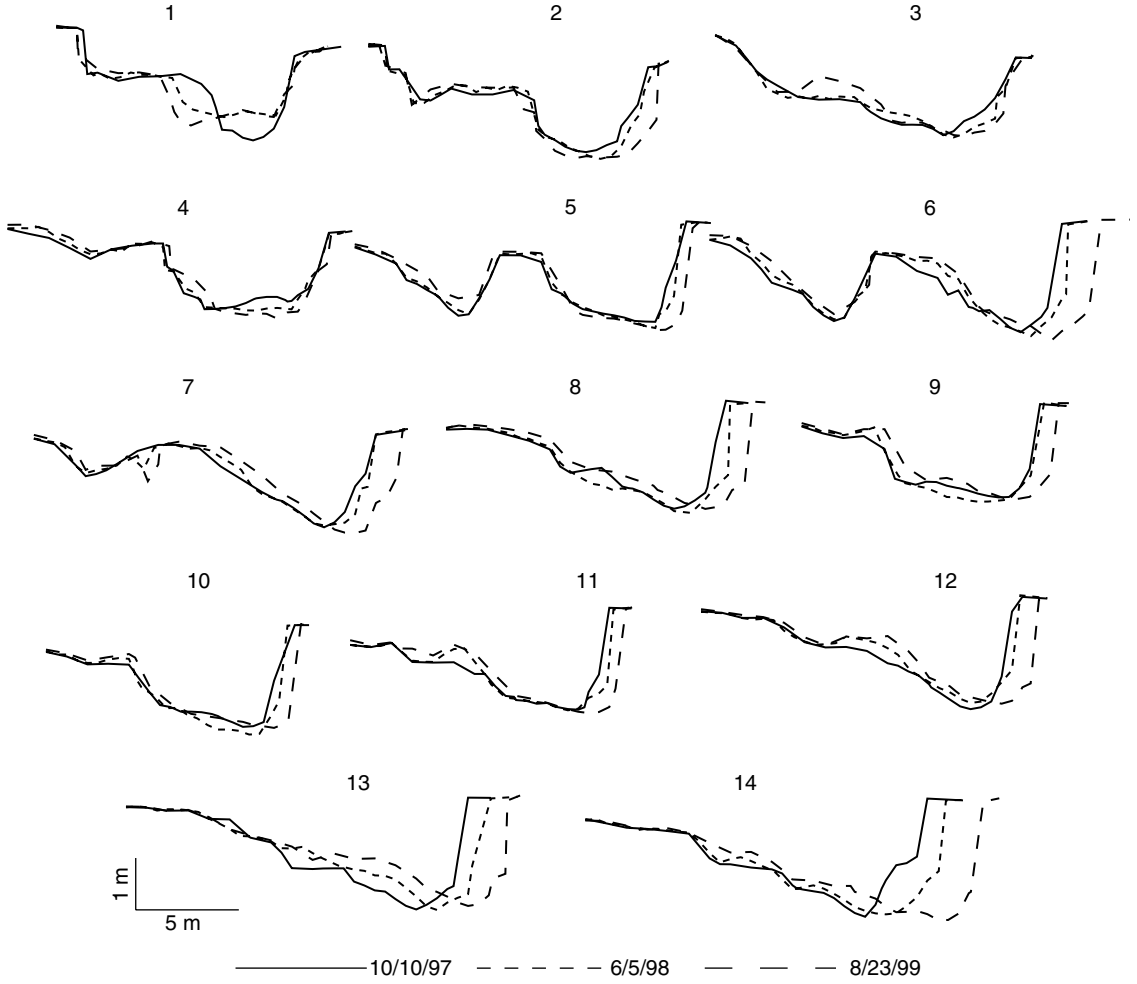

Figure 8. Changes in channel cross-sections within the compound loop between October 1997 and August 1999

the top of the inner bank at the lobe entrance (cross-sections 5 and 6) consist mainly of fine gravel, indicating that bedload is transported onto the inner surface of the loop during high flows. In the downstream lobe, vertical accumulations of sediment associated with lateral accretion are between 0·25 and 0·30 m, but most deposition occurs on the low face of the point bar (Figure 8). The result is gradual widening of the bankfull channel within the downstream lobe.

DISCUSSION

Geomorphologists have long recognized that flow in meandering streams is 3-D. However, until recently, limitations in measurement technology have prohibited the collection of 3-D velocity data and, as a result, 3-D flow structure has been inferred from 1- or 2-D data (e.g. Hickin, 1978; Dietrich and Smith, 1983; Thorne and Rais, 1984; Thorne *et al*., 1985). This study is one of the first to examine 3-D velocity fields in a meandering stream directly. The focus on 3-D velocity characteristics and patterns of channel erosion and deposition in an asymmetrical compound meander loop is novel, because previous experimental and field studies of flow structure in meandering rivers have focused mainly on bends of relatively simple geometry.

Patterns of downstream velocity through the asymmetrical compound loop along the Embarras River are similar, but not identical, to patterns observed in experimental studies of symmetrical loops (Whiting and

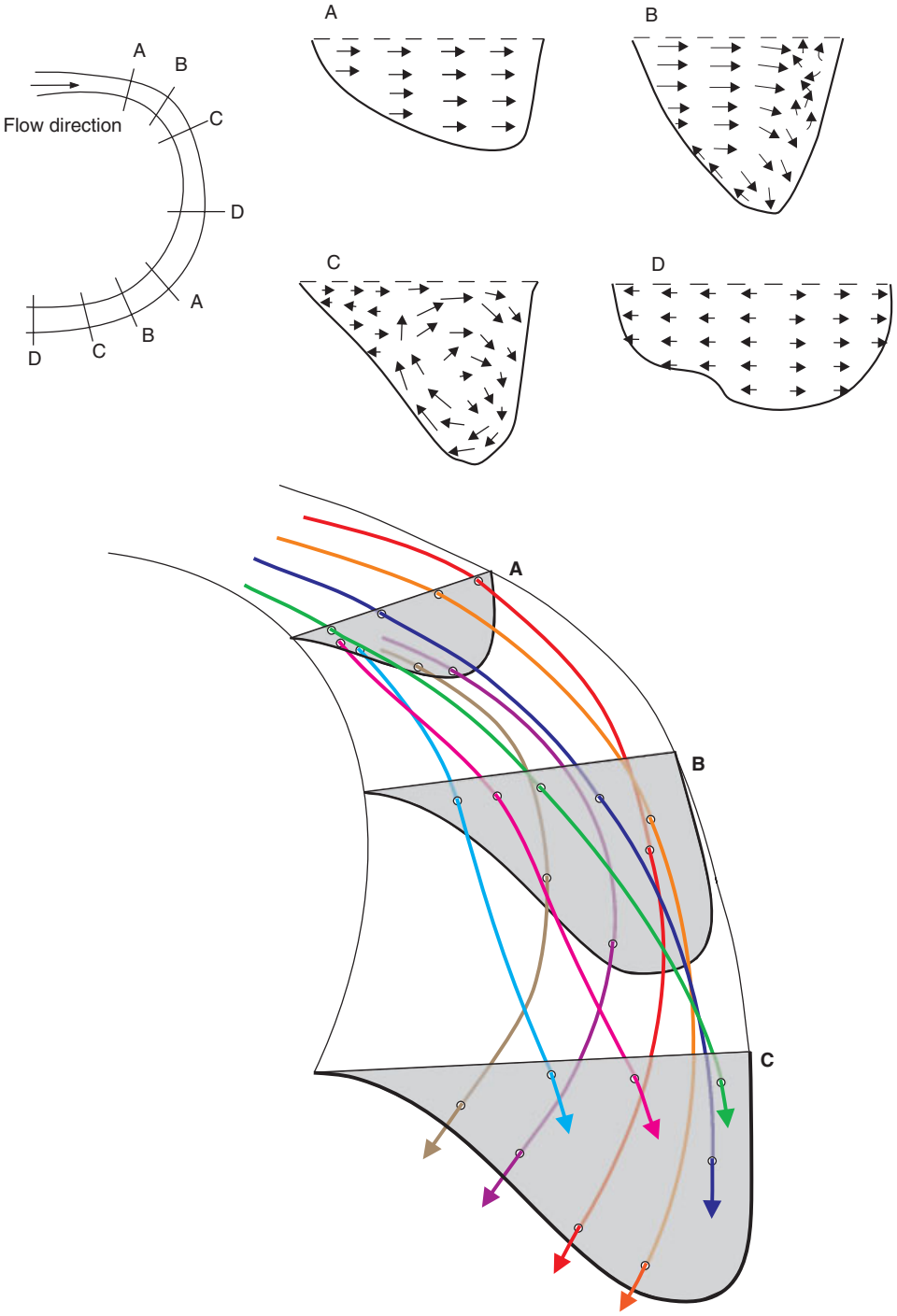

Figure 9. Top: general pattern of cross-stream velocity vectors within lobes of a compound loop. Cross-section A: outward flow over the entire cross section. Cross-section B: outward flow at surface, downward flow over thalweg, incipient inward flow along the bed. Cross-section C: fully developed helical motion. Cross-section D: replacement of decayed helicity with flow divergence. Bottom: spatial evolution of helical motion in curved lobe of a meander loop as inferred from 3-D velocity data. Near-surface streamlines in upstream part of the lobe rotate outward and downward toward the bed, whereas near-bed streamlines in the upstream part of the lobe rotate inward along the point bar face, upward toward the surface and outward over the thalweg. Because helical trajectories of streamlines are gradual and helicity decays rapidly as flow moves toward inflections in curvature, no streamline likely completes a full cycle of helical rotation within a lobe

Dietrich, 1993b). At the upstream riffle, the field data show that the high-velocity core is roughly centred in the channel cross-section (Figure 7), whereas in experimental studies the velocities are highest along the inner (right) bank at this location (Whiting and Dietrich, 1993b). Moreover, the outward shift of the high-velocity core through the pool in the upstream lobe is more pronounced for the field data than for experimental data. This discrepancy probably reflects the abrupt change in channel curvature within this lobe compared with the smooth curvature of the symmetrical experimental loop. The abrupt change in curvature of the upstream lobe (Figure 4) promotes substantial centrifugal acceleration and strong outward advection of downstream momentum. Downstream velocities decrease as flow exits the upstream pool and moves toward the second lobe, a finding consistent with Whiting and Dietrich's (1993b) results. In the downstream pool, velocities are highest along the outer bank immediately downstream of the lobe apex, a pattern consistent with that observed by Whiting and Dietrich (1993b).

The cross-stream/vertical velocity data for the compound loop indicate that, for all flow stages, helical motion occurs in the pools near the two lobe apexes and that helicity diminishes in intervening riffles. Studies based on 2-D velocity data have shown that flow in bends moves outward at the surface and inward at the bed (Bathurst *et al*., 1979; Thorne and Rais, 1984; Thorne *et al*., 1985), but vertical motion has been inferred based on the 2-D pattern of flow. The vertical velocity data collected in this study confirm that, consistent with inferences from 2-D studies (Hickin, 1978; Dietrich and Smith, 1983; Geldof and de Vriend, 1983; Thorne and Rais, 1984; Smith and McLean, 1984; Thorne *et al*., 1985; Markham and Thorne, 1992), fluid moves downward near the outer bank at the surface and inward and upward toward the inner bank near the bed.

The 3-D data also illustrate the progression of helical motion as flow moves through the lobes of a compound meander loop (Figure 9). At the entrance to the upstream lobe of a compound loop, flow throughout the cross-section is directed toward the outer concave bank with little or no vertical motion. This pattern indicates that the path of the flow does not conform to the path of the channel. Net cross-stream motion leads to the accumulation of fluid along the outer bank and the development of superelevation of the water surface and a counteracting pressure-gradient force. As flow moves into the pool near the bend apex, surface flow is oriented toward the outer bank. Near the outer bank, the outward-moving surface flow is forced downward by the adverse lateral pressure gradient associated with superelevation of the water surface, and near the bed the fluid begins to move inward and upward over the point-bar face. The outward advection of high-momentum near-surface flow toward the outer bank and vertical advection of this flow toward the bed over the thalweg shifts the core of high downstream velocity outward and downward near the base of the outer bank – a well-documented characteristic of the velocity field in meander bends (Bathurst *et al*., 1979; Thorne and Rais, 1984). As flow moves past the apex toward the pool exit, the outward and downward motion of near-surface fluid and the inward and upward motion of near-bed fluid become fully developed in a pattern of evident helicity in the cross-stream plane. As flow moves out of the lobe toward the intervening riffle, helicity breaks down and is replaced by net flow divergence (Figure 9).

The 3-D velocity data suggest that the flow completes *at most* only a single revolution of spiral motion as it moves through the lobes of the compound loop, rather than executing multiple helical revolutions (Figure 9). This finding differs from conceptual models that show fluid streamlines completing more than one helical revolution within a bend (e.g. Thompson, 1986). The data also do not exhibit definitive evidence of the small outer-bank helical cell documented in 2-D studies (Thorne and Rais, 1984; Markham and Thorne, 1992; Hey and Rainbird, 1996). The density of measurements near the outer bank in this study may not be sufficient to provide requisite information for identification of this cell. Also, the pattern of flow near the outer bank at the study site is complicated by the highly irregular topography produced by blocks of failed bank material.

The disintegration of the helical motion as flow moves out of the pool onto the downstream riffles is consistent with Thompson's (1986) conceptual model of flow through meandering channels. Disintegration of this motion may be a product of the riffle itself, or, alternatively, the riffle may mark a region of deposition associated with decay of helicity (e.g. Hooke and Harvey, 1983). Flow over the riffles is predominantly 2-D, and the velocity data do not reveal the presence of discernible vertically stacked (Thorne and Hey, 1979) or laterally adjacent (Hey and Thorne, 1975) helical cells at these locations.

Patterns of erosion and deposition within the meandering reach are generally consistent with patterns of velocity data. In the upstream lobe, maximum rates of bank retreat upstream of the lobe apex seem to be

related to impingement of the flow on the outer bank. Flow enters the upstream lobe at an oblique angle to the channel direction and cross-stream/vertical vectors indicate that strong outward fluid motion occurs close to the outer bank upstream of the lobe apex at high flows (Figure 7). Thus, the flow appears literally to collide with the outer bank in this portion of the lobe, producing a zone of strong fluid shear (clustered isovels) immediately adjacent to the outer bank (Figure 7; cross-section 6). The oblique alignment of the flow to the channel direction at the upstream-lobe entrance appears to result from patterns of erosion within the upstream limb of the loop that, in turn, are controlled by evolution of the bend upstream of this limb (e.g. Carson and Lapointe, 1983).

Flow moves through the downstream lobe roughly parallel to the channel direction and, here, maximum rates of erosion occur downstream of the lobe apex where the high-velocity core is submerged near the base of the outer bank. Although local bed shear stresses were not estimated in this study, a submerged core of high-velocity fluid produces compression of isovels near the bed, which should enhance the bed shear stress. Past work on simple meander bends has shown that large bed shear stresses occur along the outer bank immediately downstream of the bend apex (Bathurst *et al*., 1979; Dietrich *et al*., 1984) – the locus of maximum bank erosion in bends (Leopold *et al*., 1964: 299–301; Knighton, 1998: 219). This pattern of bank erosion is related to the phase lag between the flow path and channel curvature (Chang, 1988: 309–312).

The patterns of bank erosion observed at the field site are almost identical to those observed in experimental elongate loops with erodible banks that have evolved into an asymmetrical, compound form. Maximum erosion in experimental asymmetrical compound loops occurs upstream of the apex in the upstream lobe and downstream of the lobe apex in the downstream lobe (Whiting and Dietrich, 1993b: 3613). Also, the outer bank of the downstream limb of the loop erodes at the highest rate in experimental studies, leading to widening of the channel at this location and distortion of the loop geometry. The field data confirm that the highest rates of bank retreat have occurred on the outer bank of the downstream limb (Figure 8). The channel at this location is also wider than elsewhere throughout the loop (Figure 5).

The overall pattern of erosion and deposition at the field site has enhanced the asymmetry of the loop by shifting the outer bank at different rates and in different directions at upstream and downstream locations (Figure 10). This mode of evolution is consistent with the model of loop asymmetry proposed by Carson and Lapointe (1983) and with experimental results by Whiting and Dietrich (1993b). Rapid migration of the downstream limb of a symmetrical large-amplitude bend produces an asymmetric form characterized by upstream and downstream limbs of different curvature connected by a short radius of curvature minimum, or cusp. Once asymmetry is established it is preserved and enhanced by a progressive shift of the foci of maximum erosion upstream of the apex in the upstream lobe and downstream of the apex in the downstream lobe.

CONCLUSIONS

This study contributes to the understanding of the dynamics of meandering rivers by documenting 3-D time-averaged velocities and patterns of erosion and deposition in an asymmetrical compound meander loop. Major findings are that:

(1) flow in the loop is highly 3-D, but this three-dimensionality varies spatially, with skew-induced helical flow developing in pools near lobe apexes and decaying in riffles where channel curvature is less pronounced;
(2) the spatial pattern of downstream velocity generally conforms to the pattern observed in experimental symmetrical meander loops (Whiting and Dietrich, 1993a,b), but the core of high velocity at the entrance to the upstream lobe is not shifted toward the inner bank, as it is in experimental studies;
(3) maximum rates of bank retreat occur immediately upstream of the lobe apex in the upstream lobe of the loop, where flow collides with the outer bank at an oblique angle, and downstream of the lobe apex in the downstream lobe, where the high-velocity core is submerged near the base of the outer bank via advection of downstream momentum by helical motion;
(4) different rates and directions of bank erosion at the two lobes lead to increasing asymmetry of the loop geometry over time.

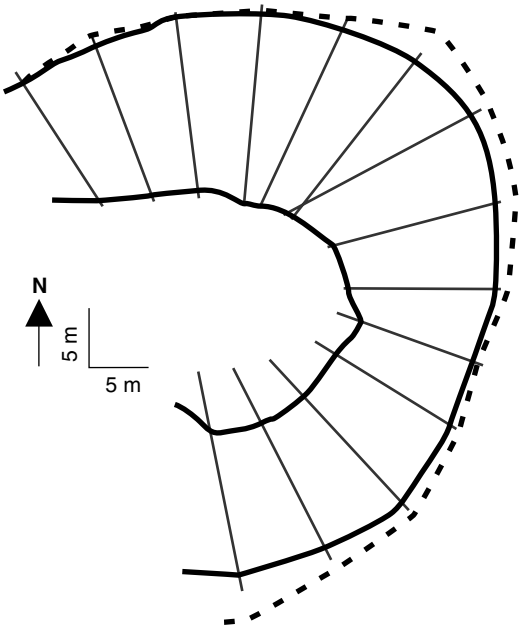

Figure 10. Pattern of bank retreat and channel migration at the study site between October 1997 and August 1999 showing evolution of loop geometry toward increasing planform asymmetry

The velocity measurements obtained in this study did not document flow structure at near-bankfull stage, when the potential for channel change via sediment transport and bank erosion is greater than at sub-bankfull stages. Although the general similarity among the 3-D velocities during measurement campaigns with different stages suggests that flow structure at bankfull stage may not differ substantively from that documented here for sub-bankfull stages, this inference needs to be verified directly. Patterns of channel change also indicate that the short-term spatial evolution of the meander loop along the Embarras River is linked to the spatial evolution of loops upstream and downstream – a finding consistent with modelling-based analysis of meander dynamics (Furbish, 1991; Stolum, 1998). Insight into spatial interaction among loops can be gained by conducting field experiments that document relations between flow structure and channel change in multiple loops.

ACKNOWLEDGEMENTS

Michael Urban, Melinda Daniels, Marta Graves, Matthew Ladewig, Perry Cabot, Alexander Sukhodolov, Nick Arnaut, Melissa Cerone, Kristin Jaburek, Kyle Landwehr, Kathleen Gregory, and Scott Rayburg assisted in the collection of geomorphological data. Peter Whiting and an anonymous reviewer provided thoughtful comments that greatly improved the final manuscript. This work was supported by grants from the National Science Foundation (SBR-9811322), the US Environmental Protection Agency (R82-5306-010), and the Department of Geography at the University of Illinois.

REFERENCES

Anon. 1980. *Webster's New World Dictionary*, 2nd College Edition. Prentice Hall: New York.

Bathurst JC, Thorne CR, Hey RD. 1979. Secondary flow and shear stress at river bends. *Journal of the Hydraulics Division, ASCE* **105**: 1277–1295.

Brice JC. 1974. Evolution of meander loops. *Geological Society of America Bulletin* **85**: 581–586.

Carson MA, Lapointe MF. 1983. The inherent asymmetry of river meander planform. *Journal of Geology* **91**: 41–56.

Chang HH. 1988. On the cause of river meandering. In *International Conference on River Regime*, White WR (ed.). John Wiley and Sons: New York; 83–93.

Dietrich WE. 1987. Mechanics of flow and sediment transport in river bends. In *River Channels Environment and Process*, Richards K (ed.). Basil Blackwell: Oxford; 179–224.

Dietrich WE, Smith JD. 1983. Influence of the point bar on flow through curved channels. *Water Resources Research* **19**: 1173–1192.
Dietrich WE, Smith JD, Dunne T. 1984. Boundary shear stress and sediment transport in river meanders of sand and gravel. In *River Meandering: Proceeding of the Conference Rivers 1983*, Elliot CM (ed.). American Society of Civil Engineers: New York; 632–639.
Frothingham KM. 2001. *Geomorphological processes in meandering and straight reaches of an agricultural stream in east central Illinois: relations to aquatic habitat*. PhD thesis, University of Illinois, Urbana.
Furbish DJ. 1991. Spatial autoregressive structure in meander evolution. *Geological Society of America Bulletin* **103**: 1576–1589.
Geldof HJ, de Vriend HJ. 1983. Distribution of main flow velocity in alternating river channels. *Special Publication of the International Association of Sedimentologists* **6**: 85–95.
Hansel AK, Johnson WH. 1992. Fluctuations of the Lake Michigan lobe during the Late Wisconsin Subepisode. *Sveriges Geologiska Undersokning, Series Ca* **81**: 133–144.
Hey RD, Rainbird P. 1996. Three-dimensional flow in straight and curved channels. In *Advances in Fluvial Dynamics and Stratigraphy*, Carling P, Dawson MR (eds). John Wiley and Sons: Chichester; 33–66.
Hey RD, Thorne CR. 1975. Secondary flows in river channels. *Area* **7**: 191–195.
Hickin EJ. 1978. Mean flow structure in meanders of the Squamish River, British Columbia. *Canadian Journal of Earth Science* **15**: 1834–1848.
Hooke JM. 1995. Processes of channel planform change on meandering channels in the UK. In *Changing River Channels*, Gurnell A, Petts G (eds). Wiley: Chichester; 87–115.
Hooke JM, Harvey AM. 1983. Meander changes in relation to bend morphology and secondary flows. *Special Publications of the International Association of Sedimentologists* **6**: 121–132.
Knighton D. 1998. *Fluvial Forms and Processes*. Edward Arnold: Oxford.
Leopold LB, Wolman MG, Miller JP. 1964. *Fluvial Processes in Geomorphology*. Freeman: San Francisco.
Markham AJ, Thorne CR. 1992. Geomorphology of gravel-bed river bends. In *Dynamics of Gravel-bed Rivers*, Billi P, Hey RD, Thorne CR, Tacconi P (eds). John Wiley & Sons: Chichester; 433–456.
Rhoads BL, Kenworthy ST. 1995. Flow structure at an asymmetrical stream confluence. *Geomorphology* **11**: 273–293.
Rhoads BL, Urban MA. 1997. Human-induced geomorphic changes in low-energy agricultural streams: an example from east-central Illinois. In *Management of Landscapes Disturbed by Channel Incision*, Wang SSY, Langendoen EJ, Shields Jr FD (eds). *The Center for Computational Hydroscience and Engineering*, The University of Mississippi: Oxford, MS; 968–973.
Rhoads BL, Welford MR. 1991. Initiation of river meandering. *Progress in Physical Geography* **15**: 127–156.
Smith JD, McLean SR. 1984. A model for flow in meandering streams. *Water Resources Research* **20**(9): 1301–1315.
Stolum H. 1998. Planform geometry and dynamics of meandering rivers. *Geological Society of America Bulletin* **110**(11): 1485–1498.
Thompson A. 1986. Secondary flows and the pool–riffle unit: a case study of the processes of meander development. *Earth Surface Processes and Landforms* **11**: 631–641.
Thorne CR, Hey RD. 1979. Direct measurements of secondary currents at a river inflexion point. *Nature* **280**: 226–228.
Thorne CR, Rais S. 1984. Secondary current measurements in a meandering river. In *River Meandering: Proceedings of the Conference Rivers 1983*, Elliot CM (ed.). American Society of Civil Engineers: New York; 675–686.
Thorne CR, Zevenbergen LW, Pitlick JC, Rais S, Bradley JB, Julien PY. 1985. Direct measurements of secondary currents in a meandering sand-bed river. *Nature* **315**: 746–747.
Urban MA. 2000. *Conceptualizing anthropogenic change in fluvial systems: drainage development on the upper Embarras River, Illinois*. PhD. thesis, University of Illinois, Urbana.
Whiting PJ, Dietrich WE. 1993a. Experimental studies of bed topography and flow patterns in large-amplitude meanders 2. Mechanisms. *Water Resources Research* **29**(11): 3615–3622.
Whiting PJ, Dietrich WE. 1993b. Experimental studies of bed topography and flow patterns in large-amplitude meanders 1. Observations. *Water Resources Research* **29**(11): 3605–3614.

